Supporting Information

Composite hydrogels with tunable anisotropic morphologies and mechanical properties

Mokit Chau[1‡], Kevin J. De France[2‡], Bernd Kopera[1,3], Vanessa R. Machado[1], Sabine Rosenfeldt[3], Laura Reyes[1], Katelyn J. W. Chan[2], Stephan Förster[3], Emily D. Cranston[2]*, Todd Hoare[2,4]*, Eugenia Ku-macheva[1,5,6]*

Atomic force microscopy imaging of aldehyde-modified CNCs

Aldehyde-modified CNCs (A-CNCs) were imaged in contact mode using an AFM in alternating current (AC) mode with an Asylum MFP-3D atomic force microscope (Asylum Research, Santa Barbara, CA). Rectangular FMR cantilevers (NanoWorld) with normal spring constants of 1.2–5.5 N/m and resonance frequencies of 60–90 kHz were used to obtain the image shown in Figure S1.

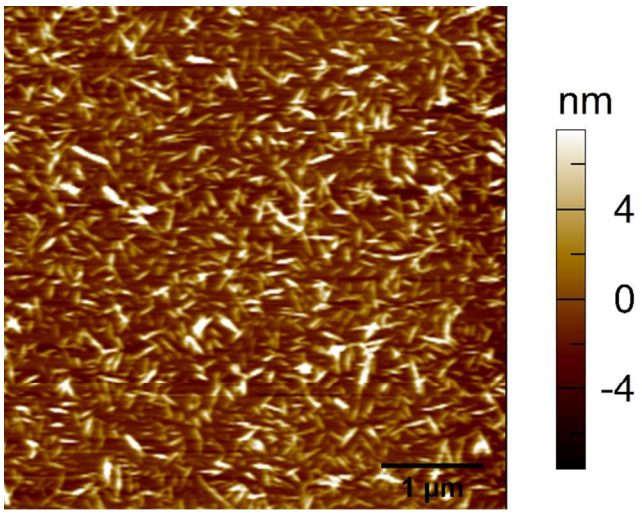

Figure S1. Atomic force microscopy height image of aldehyde-functionalized CNCs.

Experimental setup for freeze-casting at -80 to -20 °C (Assembly 2)

The setup for freeze-casting at temperature in the range from -80 to -20 °C is illustrated in Figure S2. The setup consists of an aluminum rod, 2 inches in diameter and 12 inches

in height (McMaster-Carr 8974K552), topped with six circular polyimide round heaters (Omega Product Number KHR-2/10) that are spaced by copper plates. Above the heaters is a copper cylinder, 2 inches in diameter and 1 inch in height (McMaster-Carr 9103K2). The assembly was placed in a stainless steel Dewar filled with liquid nitrogen. The temperature of the heating elements was controlled using a PID controller connected to a thermocouple inserted in the copper cylinder.

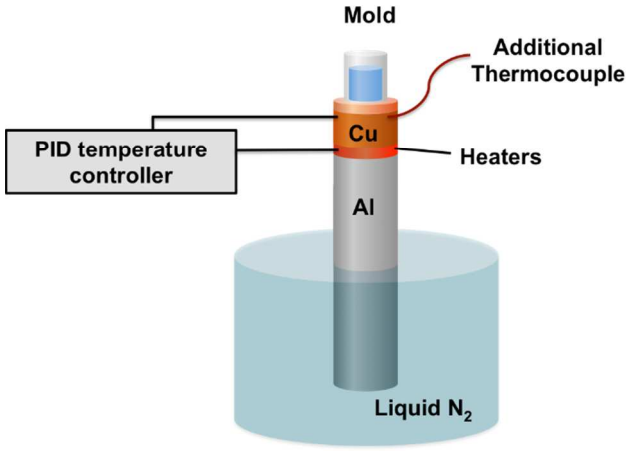

Figure S2. Experimental setup used for the preparation of aerogels at freeze-casting temperatures in the range from -80 to -20 °C.

Gelation times and freeze-casting times

The time required for freeze-casting in square molds and cylindrical molds for all samples were ~200 s and ~100 s, respectively, when the freeze-casting temperature was -196 °C. The times of gelation (in the absence of freeze-casting) of A-CNC/H-POEGMA dispersions with different compositions are shown in Table S1. Therefore, gelation started before freeze-casting and could proceed during the freeze-casting process.

Table S1. Gelation times of A-CNC:H-POEGMA dispersions (no freeze casting)

		$C_{A\text{-}CNC+H\text{-}POEGMA}$ (wt%)			
		1	2.5	4	7
Weight ratio of A-CNC:H-POEGMA	1:1	no gel	~80 s	~75 s	~40 s
	1:3	no gel	no gel	no gel	~55 s
	1:5	no gel	no gel	no gel	~60 s

The average freezing velocity was determined as the height of the sample divided by the time of its freezing. To reproduce the conditions of freeze-casting, in square and cylindrical molds, we ensured that the average freezing velocity during the freeze-casting process were the similar for the samples prepared for both the structural characterization and mechanical testing. In particular, at -196 °C, the freezing velocities for the samples prepared in the square and cylindrical molds were 0.11 and 0.09 mm/s, respectively. At -20 °C, the corresponding average freezing velocities were 0.053 and 0.032 cm/s and at –80 °C, the corresponding average freezing rates were 0.015 and 0.01 cm/s.

Freeze-casting of suspensions containing A-CNSs or H-POEGMA

In the control experiments, we freeze-cast foams from dispersions containing either only 4 wt% H-POEGMA, or only 4 wt% H-CNCs. Aerogels formed by only H-POEMGA, collapsed into a pellet after freeze-drying (Figure S3), due to the softness (low T_g) of uncrosslinked POEGMA.[3] Aerogels formed from only A-CNCs were stable after freeze-casting (Figure S4a) and exhibited a lamellar structure (Figure S4b), however upon the introduction of water, these aerogels disintegrate immediately (Figure S4c). Therefore, crosslinking of the components was important for aerogel structural integrity and hydrogel stability in water.

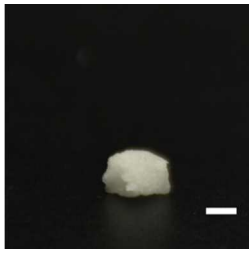

Figure S3 Photograph of the pellet that resulted from the freeze-casting of only H-POEGMA. The scale bar is 2500 µm.

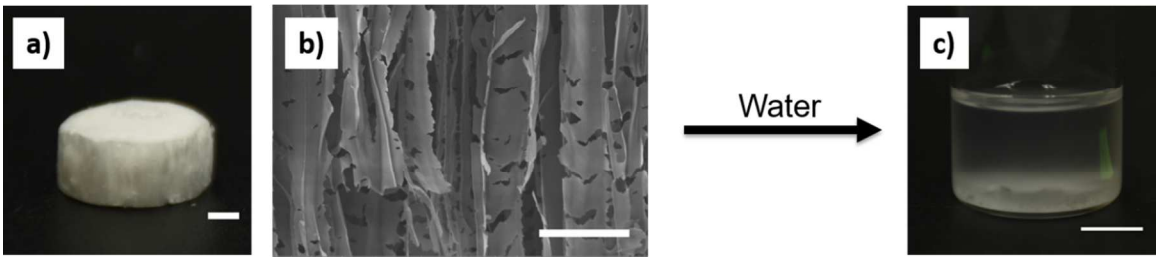

Figure S4. a) Photograph of the A-CNC aerogel. The scale bar is 2.5 mm. b) SEM image of the A-CNC aerogel. The scale bar is 50 µm.c) Photograph showing the disintegration of pure A-CNC foam upon the introduction of water. The scale bar is 10 000 µm.

Side-view cross-sectional SEM images of composite aerogels

Figure S5a and b shows side-view SEM images of 1:5-2.5 and 1:1-4 aerogels (Table 1, main text), respectively. The images show that the aerogels have anisotropic structure

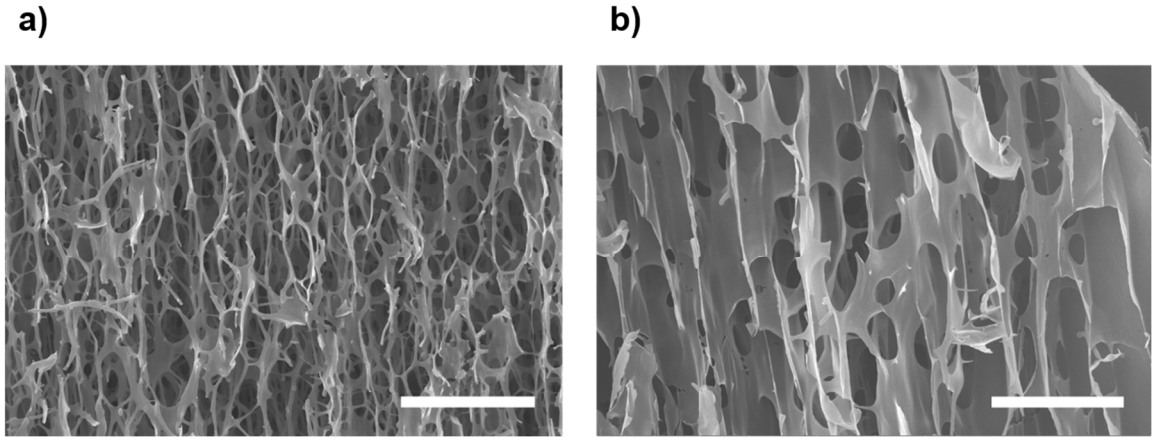

Figures S5. Side-view SEM image of a) 1:5-2.5 and b) 1:1-4 aerogels (Table 1,

main text).

SAXS patterns for aerogels of various morphologies

Figure S6 shows the 2D SAXS scattering patterns for A-CNC-H-POEGMA aerogels with different compositions irradiated in Z- and XY-direction, as well as the SEM cross-sections of the corresponding aerogels. The selected A-CNC-H-POEGMA aerogels with well-defined fibrillar (top), columnar (middle) or lamellar (bottom) mesostructures exhibited isotropic and anisotropic 2D SAXS patterns when irradiated in the Z- and XY-directions, respectively. As shown for the 1:5-4 aerogel (Table 1, main text), these patterns suggest that the mesostructures have no preferential orientation in the XY-plane, however, they are preferentially aligned in the Z-direction.

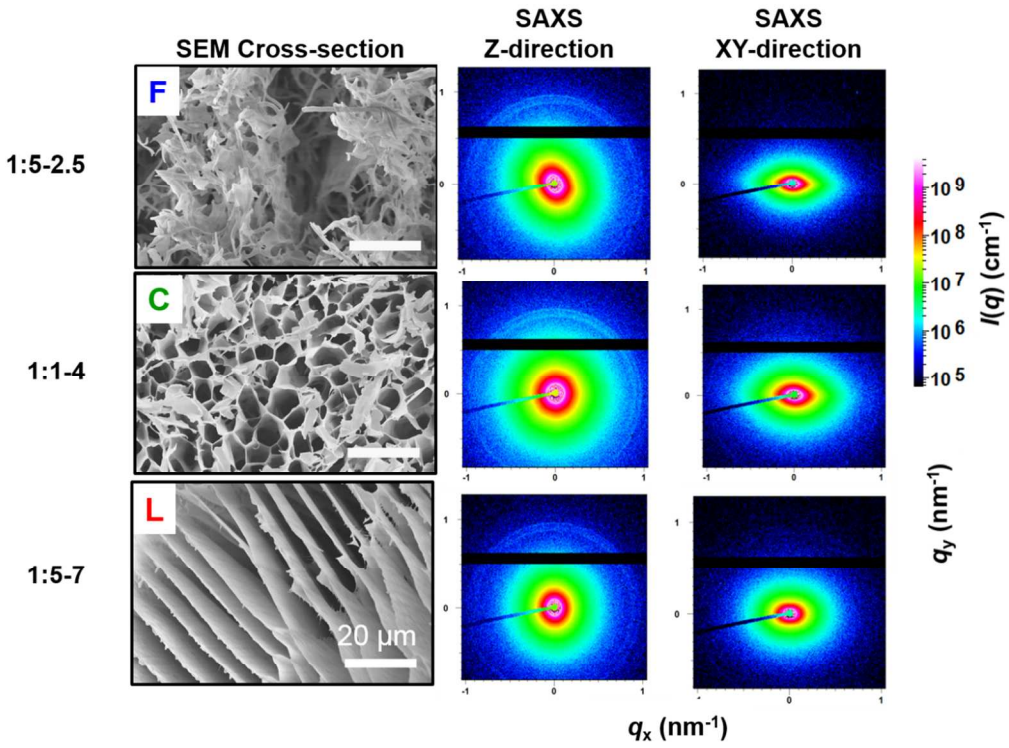

Figure S6. SEM images and corresponding 2D SAXS patterns of fibrillar (F), columnar (C), and lamellae (L) aerogels. The aerogels were irradiated in the Z- or XY-direction in SAXS experiments.

2D SAXS patterns for aerogels at high *q* values

The 2D SAXS patterns for a 1:5-4 aerogel (Table 1, main text) irradiated in the Z- and XY-directions are shown in Figure S6a and 6b, respectively. The patterns in the high *q* range, related to the scattering in crystalline CNCs, exhibited Debye-Scherrer rings, which suggested that there is no preferential orientation of the CNCs within the aerogels.

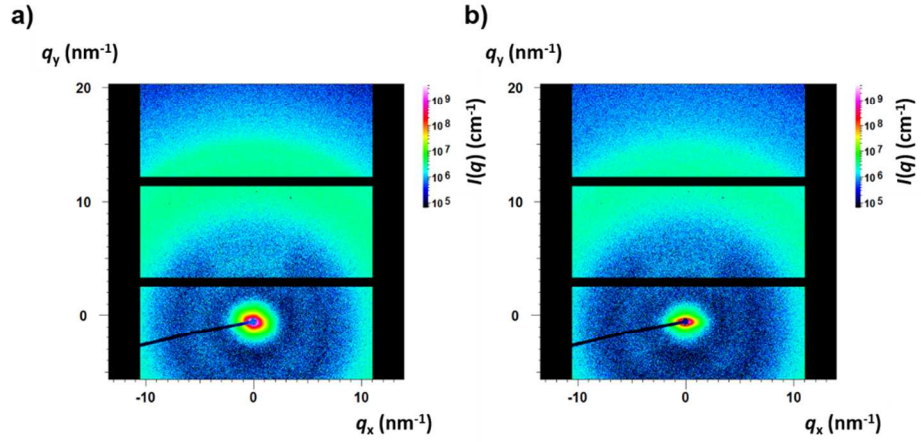

Figure S7. 2D SAXS patterns of a 1:5-4 aerogel irradiated in the (a) Z- and (b) XY-directions.

To demonstrate that Debye-Scherrer rings exist at all azimuths, Figure S8a and S7b show the 2D SAXS patterns for the 1:1-4 aerogel irradiated in Z- and XY- directions, while Figure S8c shows the 2D SAXS pattern for the same aerogel as in Figure S8b, irradiated in the same direction, after the sample was rotated by 90° about the axis parallel to the direction of irradiation. Debye-Scherrer rings were observed in all cases, which suggested that there is no alignment of the A-CNCs within the aerogels.

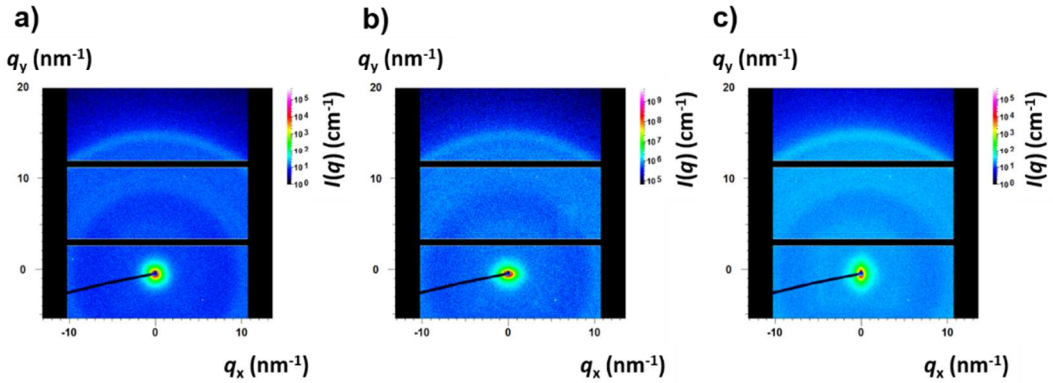

Figure S8. 2D SAXS patterns of a 1:1-4 aerogel irradiated in the (a) Z- and (b) XY-

directions. (c) 2D SAXS pattern for the same aerogel as in (b) irradiated in the same direction, except the sample was rotate by 90° about the axis parallel to the direction of irradiation.

Kinetics of hydrogel swelling

The swelling kinetics of the anisotropic hydrogel samples are shown in Figure S9. The equilibrium degree of swelling was reached for all the samples in <24 h, with a final measurement taken after 93 h.

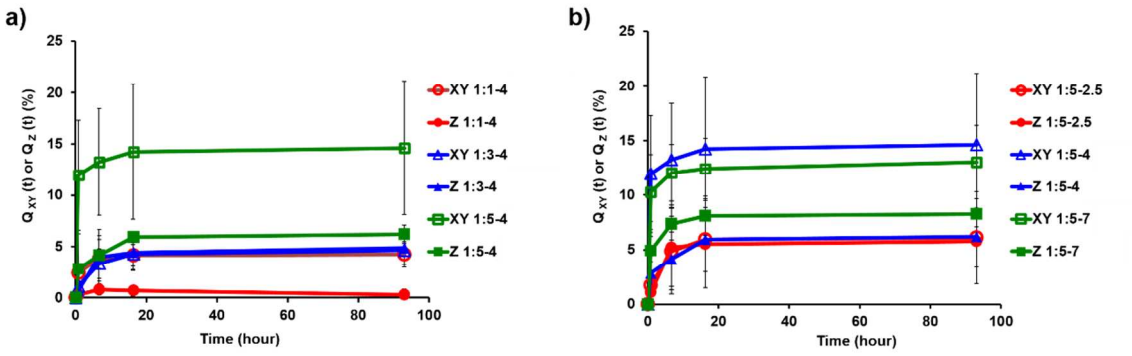

Figure S9. Swelling kinetics for A-CNC-H-POEGMA samples prepared at (a) $C_{\text{A-CNC+H-POEGMA}}$ = 4 wt% and varying A-CNC:H-POEGMA ratios and (b) at the weight ratio A-CNC:H-POEGMA of 1:5 ratio and varying $C_{\text{A-CNC+H-POEGMA}}$.

Stress-strain curves for compression of A-CNC-H-POEGMA hydrogels

Stress-strain curves for the all A-CNC-H-POEGMA hydrogels under 50 cycles of compression are shown in Figure S10.

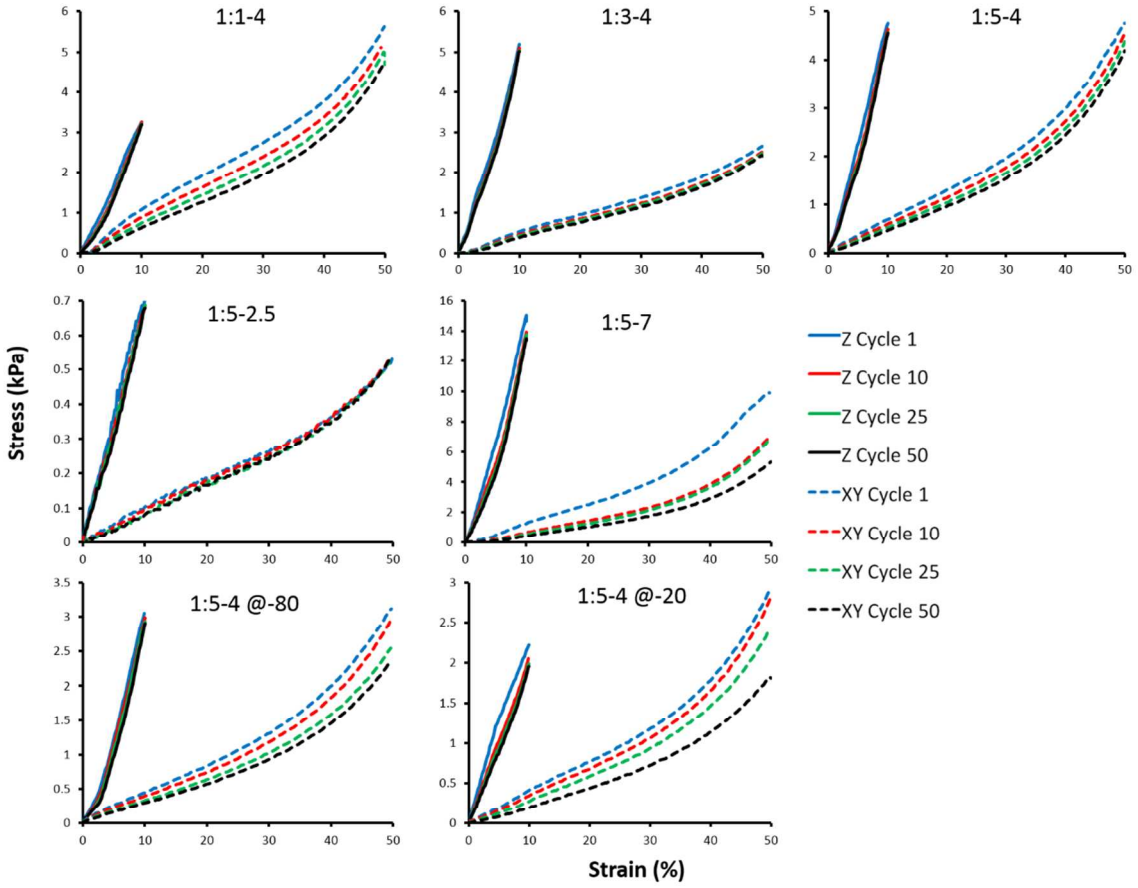

Figure S10. Stress strain curves for A-CNC-H-POEGMA hydrogels compressed parallel (Z) and perpendicular (XY) to the direction of ice growth (50 compression cycles).